Regulation of mitochondrial dynamics in acute kidney injury in cell culture and rodent models

Craig Brooks, Qingqing Wei, Sung-Gyu Cho, and Zheng Dong

Department of Cellular Biology and Anatomy, Medical College of Georgia, and Charlie Norwood VA Medical Center, Augusta, Georgia, USA.

The mechanism of mitochondrial damage, a key contributor to renal tubular cell death during acute kidney injury, remains largely unknown. Here, we have demonstrated a striking morphological change of mitochondria in experimental models of renal ischemia/reperfusion and cisplatin-induced nephrotoxicity. This change contributed to mitochondrial outer membrane permeabilization, release of apoptogenic factors, and consequent apoptosis. Following either ATP depletion or cisplatin treatment of rat renal tubular cells, mitochondrial fragmentation was observed prior to cytochrome *c* release and apoptosis. This mitochondrial fragmentation was inhibited by Bcl2 but not by caspase inhibitors. Dynamin-related protein 1 (Drp1), a critical mitochondrial fission protein, translocated to mitochondria early during tubular cell injury, and both siRNA knockdown of Drp1 and expression of a dominant-negative Drp1 attenuated mitochondrial fragmentation, cytochrome *c* release, caspase activation, and apoptosis. Further in vivo analysis revealed that mitochondrial fragmentation also occurred in proximal tubular cells in mice during renal ischemia/reperfusion and cisplatin-induced nephrotoxicity. Notably, both tubular cell apoptosis and acute kidney injury were attenuated by mdivi-1, a newly identified pharmacological inhibitor of Drp1. This study demonstrates a rapid regulation of mitochondrial dynamics during acute kidney injury and identifies mitochondrial fragmentation as what we believe to be a novel mechanism contributing to mitochondrial damage and apoptosis in vivo in mouse models of disease.

Introduction

Sublethal and lethal injury to renal tubular cells is a major intrinsic cause of acute renal failure, a disease associated with high mortality and increasing prevalence (1–9). In this condition, mitochondrial damage has been recognized as a crucial contributor to tubular cell death in both necrosis and apoptosis (1, 3, 10–14). Tubular cell necrosis may involve disruption of respiration complexes, loss of mitochondrial membrane potential, and mitochondrial permeability transition, while apoptosis is precipitated by mitochondrial outer membrane permeabilization and consequent release of apoptogenic factors such as cytochrome *c*. Recent in vivo studies have shown that ablation of proapoptotic Bcl2 family genes, such as *Bid* and *Bax*, leads to preservation of mitochondrial integrity, suppression of tubular cell apoptosis, and amelioration of ischemic and cisplatin nephrotoxic renal failure (15, 16). Notably, in humans, mitochondrial membrane permeabilization and release of cytochrome *c* seem to be key to tubular cell apoptosis in ischemically injured kidneys (17). Despite these findings, the mechanism underlying mitochondrial damage during tubular cell apoptosis remains elusive.

A new development in the understanding of mitochondrial regulation in apoptosis is the discovery of a drastic morphological change of the organelles (18, 19). Mitochondria are dynamic organelles that maintain their shape or morphology via 2 opposing processes, fission and fusion (20–22). Mitochondrial fission involves the constriction and cleavage of mitochondria by fission proteins, such as dynamin-related protein 1 (Drp1) and Fission 1 (Fis1). Mitochondrial fusion, on the other hand, is the lengthening of mitochondria by tethering and joining together 2 adjacent mitochondria. Mitofusin-1 and -2 are mainly responsible for outer membrane fusion, while Opa1 is thought to mediate inner membrane fusion (20–22). Under physiological conditions, mitochondria are elongated and filamentous. Upon stress or apoptotic stimulation, mitochondria become fragmented and, importantly, the fragmentation may contribute to mitochondrial outer membrane permeabilization and the release of apoptogenic factors from the mitochondrial intermembrane space. Thus far, mitochondrial fragmentation has been demonstrated in a variety of mammalian cells and also during programmed cell death in *Caenorhabditis elegans* and *Drosophila* (18, 19). A role for mitochondrial fragmentation in apoptosis has been suggested by notable studies but has also been seriously challenged recently by others (23–25). Critically, evidence for the occurrence of mitochondrial fragmentation and its involvement in relevant pathological or disease conditions is scarce (26).

In the current study, we have demonstrated compelling evidence for mitochondrial fragmentation in acute kidney injury using in vitro and in vivo experimental models. The fragmentation involves the activation of mitochondrial fission via Drp1. Importantly, in both cell cultures and whole animals, suppression of Drp1 and mitochondrial fragmentation abrogates mitochondrial damage, cytochrome *c* release, apoptosis, and renal injury. Regulation of mitochondrial dynamics may offer a novel strategy for the prevention and treatment of acute renal failure.

Results

Mitochondrial fragmentation occurs in response to apoptotic stress in rat proximal tubular cells. Renal ischemia and nephrotoxicity are the major causes of acute kidney injury. To examine mitochondrial morpho-

Authorship note: Craig Brooks and Qingqing Wei contributed equally to this work.

Conflict of interest: The authors have declared that no conflict of interest exists.

Nonstandard abbreviations used: BUN, blood urea nitrogen; DN-Drp1, dominant-negative Drp1; Drp1, dynamin-related protein 1; Fis1, Fission 1; PUMA-α, p53-upregulated modulator of apoptosis α; RPTC, rat proximal tubular cell; VAD, carbobenzoxy-valyl-alanyl-aspartyl-(O-methyl)-fluoromethylketone.

Citation for this article: *J. Clin. Invest.* **119**:1275–1285 (2009). doi:10.1172/JCI37829.

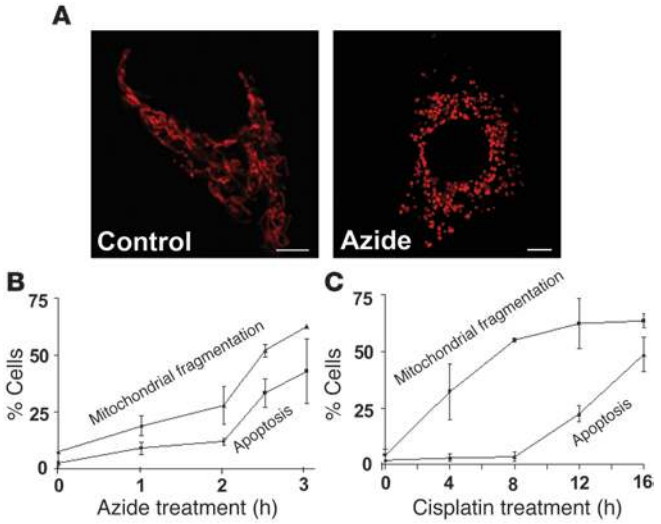

Figure 1
Mitochondrial fragmentation following ATP depletion and cisplatin treatment in RPTCs. RPTCs were transfected with MitoRed to fluorescently label mitochondria. The cells were then incubated with 10 mM azide in glucose-free medium to induce ATP depletion or treated with 20 μM cisplatin in cell culture medium. Mitochondrial morphology in MitoRed-labeled cells was evaluated by fluorescence microscopy to determine the percentage of cells that fragmented mitochondria. Apoptosis was assessed in these cells by cellular and nuclear morphology. (**A**) Representative images of mitochondrial morphology. Left panel, an untreated control RPTC showing long filamentous mitochondria with a thread-like appearance. Right panel, an azide-treated (3 hours) cell showing shortened punctate mitochondria. Scale bars: 5 μm. (**B**) Time courses of mitochondrial fragmentation and apoptosis during azide-induced ATP depletion. (**C**) Time courses of mitochondrial fragmentation and apoptosis during cisplatin incubation. Data in **B** and **C** are presented as mean ± SD; $n = 3$.

logical changes under this condition, we transfected MitoRed into cultured rat proximal tubular cells (RPTCs) to label mitochondria with red fluorescence. The cells were subsequently subjected to azide-induced ATP depletion to model in vivo ischemia or cisplatin treatment for nephrotoxicity. As shown in Figure 1A, mitochondria in control cells were filamentous with a tubular or thread-like appearance and were often interconnected to form a network. During azide treatment, the mitochondrial network broke down and the mitochondria were fragmented into short rods or spheres. Mitochondrial fragmentation was azide-treatment time dependent, concurring with apoptosis (Figure 1B). Cisplatin also induced mitochondrial fragmentation in RPTCs in a time-dependent manner (Figure 1C). Notably, mitochondrial fragmentation during cisplatin treatment clearly preceded apoptosis and, as a result, fragmentation was observed at 4 hours, whereas apoptosis was not detected until 12 hours (Figure 1C). A time-lapse study further recorded mitochondrial fragmentation during azide-induced cell injury. A very rapid/sudden fragmentation of all mitochondria in individual cells was shown after about 2 hours of azide treatment (Supplemental Video 1; supplemental material available online with this article; doi:10.1172/JCI37829DS1). The results demonstrate an early and striking morphological change of mitochondria during tubular cell injury.

Mitochondrial fragmentation can be inhibited by Bcl2 but not by caspase inhibitors. While mitochondrial fragmentation could play a causative role in mitochondrial injury and apoptosis, it may also be a result of cell death. We therefore tested the effects of carbobenzoxy-valyl-alanyl-aspartyl-(O-methyl)-fluoromethylketone (VAD), a pan-caspase inhibitor that blocks apoptosis during ATP depletion and cisplatin treatment of RPTCs. Although caspase activation and apoptosis were inhibited (not shown), VAD did not suppress mitochondrial fragmentation during either azide or cisplatin treatments (Figure 2, A and B), suggesting that mitochondrial fragmentation is not secondary to caspase activation. We further tested the effects of Bcl2 on mitochondrial fragmentation during RPTC apoptosis. As shown in Figure 2, mitochondrial fragmentation induced by azide and cisplatin was suppressed in Bcl2-transfected cells. For example, azide treatment induced mitochondrial fragmentation in 70% of RPTCs, which was reduced to 20% in Bcl2-overexpressing RPTCs (Figure 2A). Interestingly, Bcl2 but not VAD attenuated azide-induced mitochondrial permeabilization, reflected by lower cytochrome *c* release into cytosol (Figure 2C). The results suggest that Bcl2 may protect against mitochondria injury and apoptosis in part by suppressing mitochondrial fragmentation.

Drp1 is activated and translocates to mitochondria early during azide-induced ATP depletion. The morphology of mitochondria is determined by 2 opposing processes, fission and fusion (20–22). Accordingly, mitochondrial fragmentation observed in our study could be a result of activated fission, suppressed fusion, or both. We demonstrated the activation of Drp1, a fission protein, during azide treatment of RPTCs. As shown in Figure 3A, compared with untreated cells, 1–3 hours of azide treatment induced an accumulation of Drp1 in the mitochondrial fraction. Azide-induced Drp1 translocation was also confirmed by dual immunofluorescence staining of Drp1 and Fis1, an integral mitochondrial protein involved in fission (20–22). As shown in Figure 3B, colocalization in Drp1 and Fis1 was shown in some azide-treated cells. Of note, consistent with previous reports (27, 28), Drp1 appeared to be restricted to specific sites along the mitochondrial membrane, where fission may have been occurring.

Dominant-negative Drp1 inhibits mitochondrial fragmentation during RPTC injury. To determine whether Drp1 is indeed involved in mitochondrial fragmentation during tubular cell apoptosis, we tested the effects of dominant-negative Drp1 (DN-Drp1) that had a K38A point mutation (28). RPTCs were transfected with DN-Drp1 or empty vector and then treated with azide or cisplatin. As shown in Figure 4A, DN-Drp1 reduced mitochondrial fragmentation from 64% to 28% during azide treatment. Similarly, DN-Drp1 significantly inhibited mitochondrial fragmentation during cisplatin incubation (Figure 4B). Representative images are shown in Figure 4C. Untreated cells had typical filamentous mitochondria; after azide treatment, the mitochondria became fragmented and punctate, but the cells transfected with DN-Drp1 retained their filamentous mitochondria. These data suggest a role for Drp1 and associated fission in mitochondrial fragmentation during tubular cell apoptosis.

Inhibition of cytochrome c release during RPTC injury by DN-Drp1. Next, we determined whether blocking mitochondrial fragmentation with DN-Drp1 would inhibit cytochrome *c* release. RPTCs were cotransfected with MitoRed and DN-Drp1 or empty vector and then subjected to azide-induced ATP depletion. Cytochrome *c*

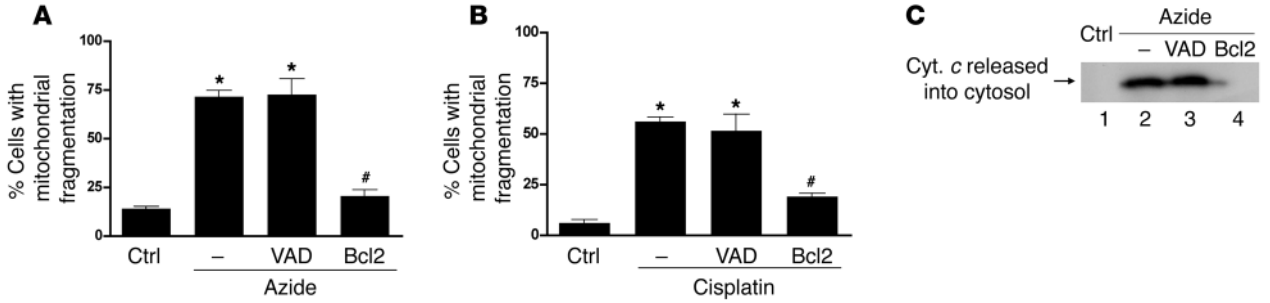

Figure 2
Inhibition of mitochondrial fragmentation and membrane permeabilization by Bcl2 and not by VAD. Wild-type and Bcl2-overexpressing RPTCs were transfected with MitoRed to label mitochondria. The cells were then treated with azide (10 mM, 3 hours) or cisplatin (20 μM, 16 hours) in the absence or presence of 100 μM VAD. Mitochondrial morphology in individual cells was evaluated by fluorescence microscopy to determine the percentage of cells with mitochondria fragmentation. (**A**) Mitochondrial fragmentation during azide-induced ATP depletion. (**B**) Mitochondrial fragmentation during cisplatin incubation. (**C**) Cytochrome *c* (Cyt. *c*) release during azide treatment. Cells were fractionated to collect cytosolic fraction for immunoblot analysis of cytochrome *c*. Data in **A** and **B** are presented as mean ± SD; $n \geq 3$. $^{*}P < 0.05$, significantly different from untreated control; $^{\#}P < 0.05$, significantly different from azide- or cisplatin-treated RPTCs. Results show that Bcl2 (but not caspase inhibitors) can suppress mitochondrial fragmentation and outer membrane permeabilization. Ctrl, control.

release was examined by immunofluorescence. Of note, the transfection efficacy in RPTCs was 20%–30%. Thus, our examination was focused on the transfected (MitoRed labeled) cells to determine the effects of DN-Drp1. Representative images are shown in Figure 5A. In control cells, cytochrome *c* was sequestered in mitochondria and overlapped with the MitoRed signal. After azide treatment, mitochondria became fragmented and cytochrome *c* was released from mitochondria and distributed throughout the cytosol. However, DN-Drp1–transfected cells retained filamentous mitochondria and maintained cytochrome *c* in the organelles. Cell counting showed that DN-Drp1 significantly inhibited cytochrome *c* release during azide treatment, reducing cytochrome *c*–released cells from 61% to 26% (Figure 5B). In contrast, DN-Drp1 did not suppress azide-induced Bax accumulation in mitochondria (Figure 5C). The results suggest that Drp1-mediated mitochondrial fragmentation contributes to mitochondrial damage and cytochrome *c* release, although it does not affect initial Bax activation or translocation.

Inhibition of RPTC apoptosis by DN-Drp1. Once released, cytochrome *c* activates caspases to result in apoptosis (29). By blocking mitochondrial fragmentation and cytochrome *c* release (Figures 4 and 5), DN-Drp1 was expected to inhibit caspase activation and apoptosis. To test this, we cotransfected RPTCs with GFP and wild-type Drp1, DN-Drp1, or empty vector. The cells were then subjected to azide treatment followed by recovery in normal medium to analyze apoptosis and caspase activation. By TUNEL assay, azide induced 51% apoptosis in vector-transfected cells, which was decreased to 27% in DN-Drp1–transfected cells (Figure 6A). Consistently, DN-Drp1 suppressed the development of apoptotic morphology in transfected (GFP-labeled) cells, including cellular shrinkage and nuclear fragmentation (Figure 6B). DN-Drp1 also suppressed caspase activation (not shown). In addition, DN-Drp1 reduced cisplatin-induced apoptosis from 55% to 32% (Figure 6C).

siRNA knockdown of Drp1 blocks mitochondrial fragmentation, cytochrome c release, and apoptosis. We further confirmed the role of Drp1 in mitochondrial regulation and apoptosis by using an RNA interference approach. Stable Drp1-siRNA cell lines, including R3 and R24, were generated by transfection of RPTCs with a specific short hairpin siRNA of Drp1 (30). Drp1 knockdown in R3 and R24 cells was verified by immunoblot analysis (Figure 7A). In response to azide treatment, both R3 and R24 cells showed significantly lower mitochondrial fragmentation than parental RPTCs (Figure 7B). Moreover, these cells demonstrated less apoptosis and cytochrome *c*

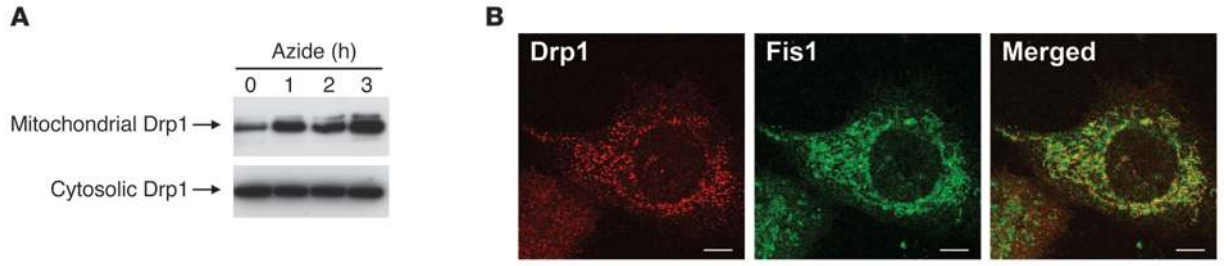

Figure 3
Drp1 translocation to mitochondria during azide-induced ATP depletion. (**A**) Immunoblot analysis of Drp1 in mitochondrial and cytosolic fractions. RPTCs were subjected to 0 to 3 hours of 10 mM azide treatment for ATP depletion and then fractionated into mitochondrial and cytosolic fractions for immunoblot analysis of Drp1. (**B**) Dual immunofluorescence staining of Drp1 and Fis1 in azide-treated cells. After 3 hours of ATP depletion by azide treatment, RPTCs were fixed for immunofluorescence of Drp1 and Fis1. Drp1 and Fis1 signals were examined by confocal microscopy, and both separate and merged images are shown. The results show the translocation of a portion of Drp1 to mitochondria, overlapping with Fis1 during ATP depletion. Scale bars: 5 μm.

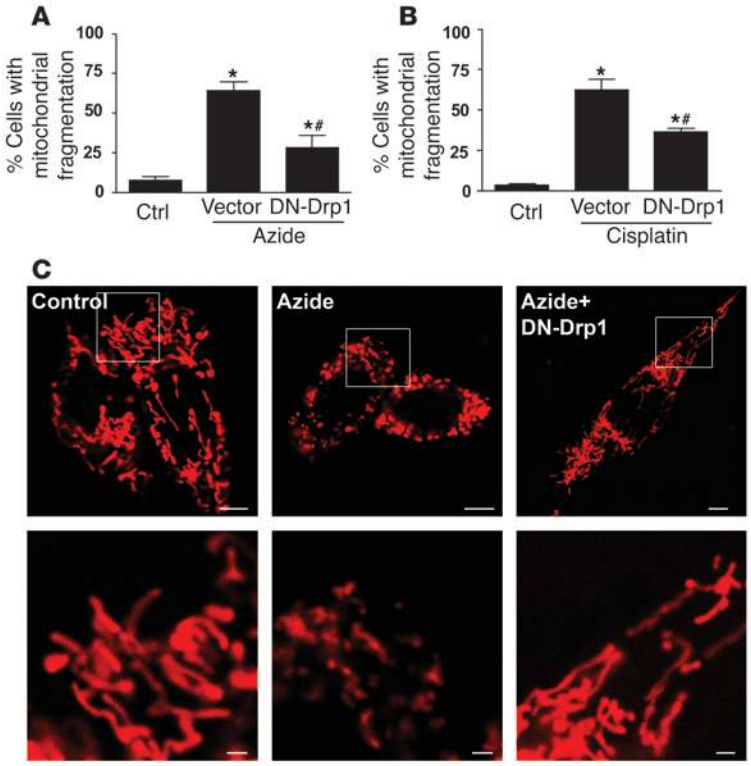

Figure 4
Suppression of mitochondrial fragmentation during RPTC injury by DN-Drp1. RPTCs were cotransfected with MitoRed and DN-Drp1 or empty vector. Cells were then incubated with 10 mM azide for 3 hours or 20 μM cisplatin for 16 hours. (**A**) Effects of DN-Drp1 on mitochondrial fragmentation during azide-induced ATP depletion. (**B**) Effects of DN-Drp1 on mitochondrial fragmentation during cisplatin treatment. (**C**) Representative images of mitochondria. Left upper panel, untreated control cells showing long thread-like filamentous mitochondria; middle upper panel, fragmented mitochondria in vector-transfected cells after azide treatment; right upper panel, cells transfected with DN-Drp1 retaining filamentous mitochondria after azide treatment. Higher-magnification images of the framed areas are shown in the bottom panels. Scale bars: 5 μm (upper panels); 1 μm (lower panels). Data in **A** and **B** are presented as mean ± SD; $n \geq 3$. $^{*}P < 0.05$, significantly different from untreated control; $^{\#}P < 0.05$, significantly different from treated group transfected with empty vector.

release (Figure 7, C and D). Cisplatin-induced mitochondrial fragmentation, cytochrome *c* release, and apoptosis were also suppressed in these cells (data not shown).

Mitochondrial fragmentation and apoptosis in primary proximal tubular cells are inhibited by DN-Drp1. To further substantiate the role of mitochondrial fragmentation in renal injury, we examined mitochondrial fragmentation during cisplatin treatment of primary proximal tubular cells. Primary cultures of proximal tubular cells had highly filamentous mitochondria (Figure 8A). Upon cisplatin treatment, however, the mitochondria became fragmented and punctate (Figure 8A). The fragmentation was inhibited by DN-Drp1 (Figure 8A). Cell counting indicated that DN-Drp1 reduced mitochondrial fragmentation from 55% to 31% (Figure 8B). DN-Drp1 also suppressed cisplatin-induced apoptosis in the primary cells (Figure 8C). To determine whether Drp1 suppression affects upstream signaling during cisplatin treatment, we examined cisplatin-induced p53 phosphorylation and p53-upregulated modulator of apoptosis α (PUMA-α) induction (31) in RPTCs stably transfected with Drp1 siRNA. Downregulation of Drp1 in the siRNA cells was verified above, as shown in Figure 7A. As shown in Supplemental Figure 1, Drp1 siRNA cells showed p53 and PUMA-α induction similar to that of the parental wild-type RPTCs, suggesting that Drp1 suppression does not affect upstream signaling during cisplatin treatment. Together, these data strongly support a role for Drp1-mediated mitochondrial fragmentation in tubular cell apoptosis.

Mitochondrial fragmentation occurs in vivo in proximal tubular cells following renal ischemia. To examine mitochondrial fragmentation in vivo, C57BL/6 mice were subjected to 30 minutes of bilateral clamping to induce renal ischemia followed by brief (15 minutes) reperfusion. Kidneys were collected for EM. EM micrographs of proximal tubular cells from both cortex and outer stripe of outer medulla were selected for evaluation. Due to the orientation of mitochondria, proximal tubular cells from control animals usually displayed 10%–20% long (≥ 2 μm) filamentous mitochondria at the basal lateral side, whereas the perinuclear mitochondria were cross-sectioned and thus appeared "fragmented" (Figure 9A). After ischemia/reperfusion, however, many proximal tubular cells completely fragmented their mitochondria into small, punctate suborganelles (Figure 9A). For quantification, we determined the percentage of cells that had completely lost their long mitochondria. As shown in Figure 9B, sham control had approximately 7% proximal tubular cells with fragmented mitochondria, which was increased to 42% during renal ischemia/reperfusion.

To confirm mitochondrial fragmentation in ischemically injured tubular cells, we performed 3D reconstruction of mitochondria from 100 serial section EM micrographs. The control tubular cell showed many filamentous mitochondria at the basolateral side in 2D EM (not shown); in the reconstruction, we purposely selected a perinuclear area where mitochondria appeared "fragmented" (Figure 10A). The 3D image showed clearly that these mitochondria were actually long and filamentous (Figure 10B). In sharp contrast, mitochondria in the ischemic cells were completely fragmented (Figure 10, C and D). These data indicate that mitochondrial fragmentation indeed occurs in vivo in renal tubular cells during ischemic injury.

Amelioration of ischemic and cisplatin nephrotoxic renal injury and tubular apoptosis by mdivi-1, a pharmacological inhibitor of Drp1. Cassidy-Stone and colleagues have recently screened several chemical libraries and identified mdivi-1 as an efficacious inhibitor of mitochondrial division that operates by selectively inhibiting Drp1 (32). To determine the role of Drp1 and mitochondrial fragmentation in vivo, we examined the effects of mdivi-1 in the mouse model of ischemia/reperfusion (Figure 11). Ischemia/reperfusion induced a rapid loss of renal

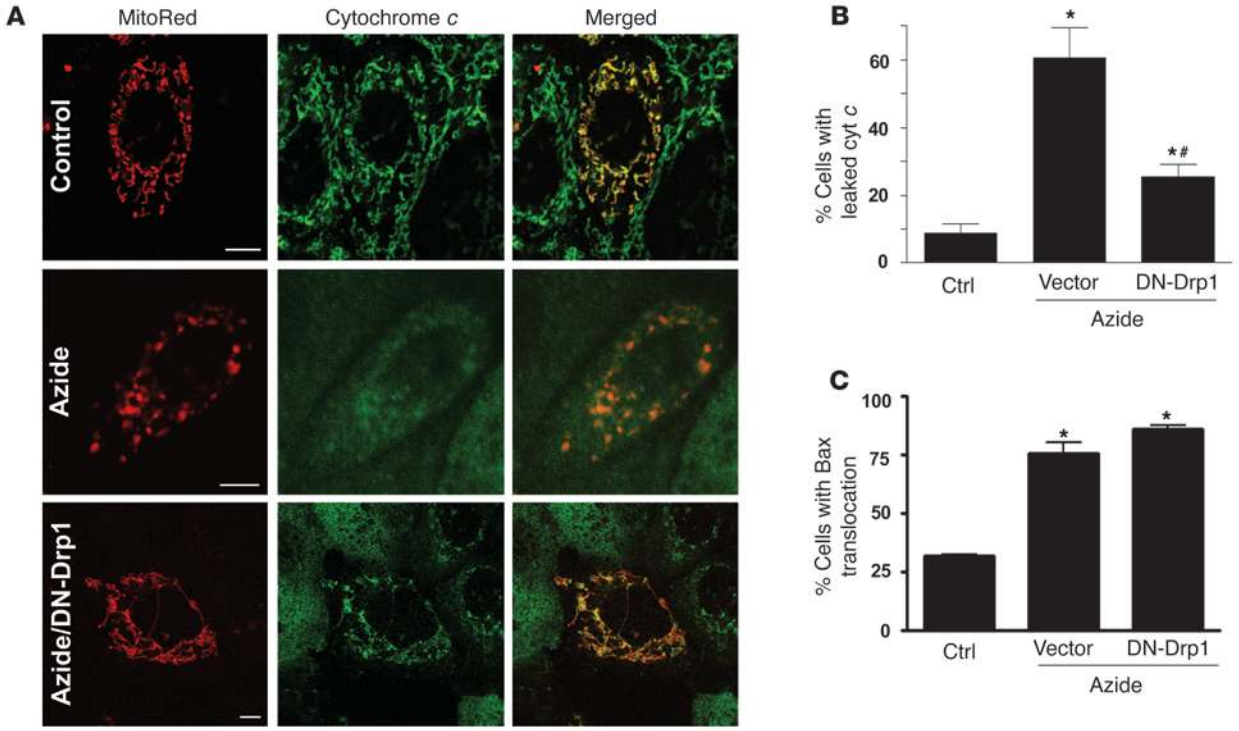

Figure 5

Inhibition of cytochrome *c* release during ATP depletion by DN-Drp1. RPTCs were cotransfected with MitoRed and DN-Drp1 or empty vector and then treated with 10 mM azide for 3 hours. The cells were fixed for immunofluorescence of cytochrome *c* or Bax. The examination was focused on the transfected (MitoRed labeled) cells to determine the effects of DN-Drp1. (**A**) Representative images of MitoRed and cytochrome *c* staining. The staining was examined by confocal microscopy in the same cells. In untreated cells (control), cytochrome *c* staining colocalized with MitoRed in filamentous mitochondria. Following azide treatment, mitochondria in vector-transfected cells became fragmented and cytochrome *c* was released into the cytosol. Cells transfected with DN-Drp1 retained their filamentous mitochondria, and cytochrome *c* was retained in mitochondria. Scale bars: 5 μm. (**B**) Quantification of the effects of DN-Drp1 on cytochrome *c* release. The localization of cytochrome *c* in MitoRed-transfected cells was evaluated to determine the percentage of cells that released cytochrome *c* into cytosol. (**C**) Quantification of the effects of DN-Drp1 on Bax translocation to mitochondria. The localization of Bax in MitoRed-transfected cells was evaluated to determine the percentage of cells that showed Bax accumulation in mitochondria. Data in **B** and **C** are presented as mean ± SD; $n \geq 3$. $^{*}P < 0.05$, significantly different from untreated control; $^{\#}P < 0.05$, significantly different from azide-treated cells that were transfected with empty vector.

function, as indicated by increases in serum creatinine and blood urea nitrogen (BUN) (Figure 11, A and B), which was partially but significantly reduced in animals pretreated with mdivi-1 (Figure 11, A and B). Consistently, mdivi-1 ameliorated tubular damage in renal cortical and outer medulla tissues, as determined by histological examination (Figure 11, C and D). We further analyzed renal apoptosis by TUNEL assay. Cell counting showed that ischemia/reperfusion induced 24 apoptotic cells/mm^2 renal tissue in mice that were pretreated with vehicle solution but only 11 in mdivi-1–pretreated mice (Figure 11E). Using EM, we confirmed that mdivi-1 partially suppressed ischemia-induced mitochondrial fragmentation in proximal tubular cells, from 43% to 32%.

We further analyzed mitochondrial fragmentation in a mouse of cisplatin nephrotoxicity (15, 33). It was shown that cisplatin (30 mg/kg) treatment for 3 and 4 days led to mitochondrial fragmentation in 33% and 53% of proximal tubular cells, respectively. We then determined the effects of mdivi-1 on cisplatin-induced renal injury and nephrotoxicity. As shown in Supplemental Figure 2, both BUN and serum creatinine increases during cisplatin treatment were reduced by daily mdivi-1 injections. Consistently, mdivi-1 ameliorated renal tissue damage, especially in renal tubules. Cisplatin-induced apoptosis was also decreased by mdivi-1 (Supplemental Figure 2). Collectively, the results support an important role for Drp1-mediated mitochondrial fragmentation in the pathogenesis of both ischemic and nephrotoxic acute kidney injury.

Discussion

Tubular cell apoptosis via the mitochondrial pathway contributes to ischemic as well as nephrotoxic acute kidney injury (1, 3, 4, 6, 10, 11, 13, 14). The inference has been supported not only by in vitro cell culture and in vivo animal studies but also by biopsy of ischemically injured human kidneys (17). In this condition, Bax and Bak are activated and form oligomers on mitochondria, leading to permeabilization of the outer membrane and release of apoptogenic factors such as cytochrome *c*. Despite these findings, it is not entirely clear how the outer membrane of mitochondria is permeabilized. In this study, we have revealed a striking morphological change of mitochondria in both in vitro and in vivo experimental models of acute kidney injury. Mitochondria become fragmented early during renal cell injury. Importantly, prevention of mitochondrial fragmentation by use of genetic and pharmacological approaches abrogates mitochondrial damage, tubular cell apoptosis, and renal injury.

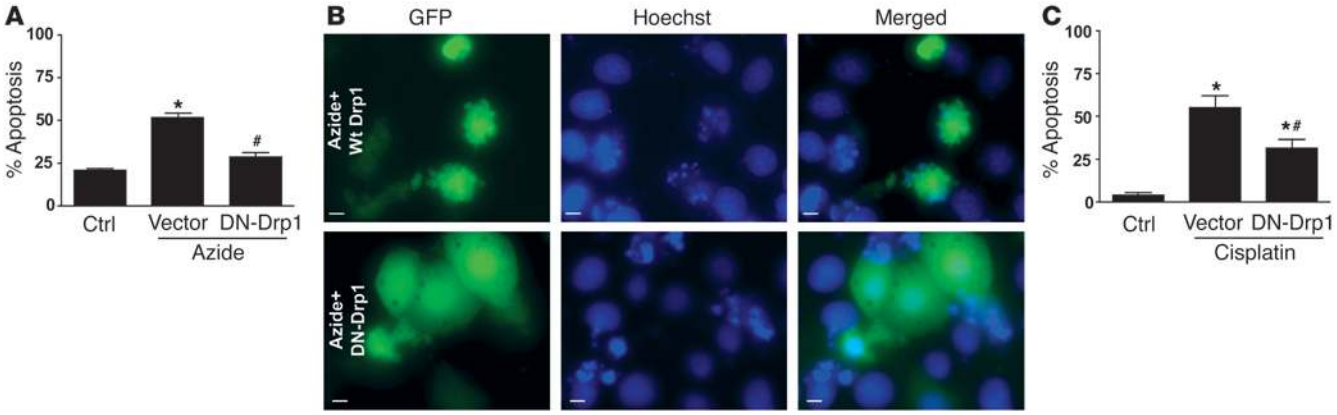

Figure 6

Inhibition of ATP depletion–induced apoptosis by DN-Drp1. (**A**) Effects of DN-Drp1 on azide-induced apoptosis. RPTCs were cotransfected with GFP and DN-Drp1 or empty vector. Cells were then treated with 10 mM azide for 3 hours followed by 2 hours recovery. After treatment, cells were subjected to TUNEL assay. Cells were examined by fluorescence microscopy to determine the percentage of apoptosis (TUNEL positive) in transfected (GFP labeled) cells. (**B**) Representative cell morphology. RPTCs were transfected with wild-type or DN-Drp1 and then subjected to 3 hours of azide treatment followed by 2 hours recovery. Cells were stained with Hoechst 33342 and examined by fluorescence microscopy. Scale bars: 5 μm. (**C**) Effects of DN-Drp1 on cisplatin-induced apoptosis. RPTCs were cotransfected with GFP and DN-Drp1 or empty vector and then incubated with 20 μM cisplatin for 16 hours. Cells were stained with Hoechst 33342 for examination by fluorescence microscopy to determine the percentage of apoptosis in transfected (GFP labeled) cells. Data in **A** and **C** are presented as mean ± SD; $n \geq 3$. $^{*}P < 0.05$, significantly different from untreated control; $^{\#}P < 0.05$, significantly different from vector-transfected cells treated with azide or cisplatin.

A role for mitochondrial fragmentation in apoptosis has been suggested and supported by notable studies (18); however, it has also been seriously challenged by others (24, 34). For example, the latest work by Sheridan et al. showed that Bcl-xL and Mcl1, 2 antiapoptotic Bcl2 family proteins, can antagonize cytochrome *c* release without blocking mitochondrial fragmentation in HeLa cells, suggesting a separation of the morphological change from mitochondrial damage (25). Breckenridge et al. further demonstrated that regulation of mitochondrial morphological dynamics does not have a significant role in the regulation of programmed cell death in *C. elegans* (23), disputing the previous finding by Jagasia et al. (35). The contrasting results may certainly be caused by differences in the experimental conditions or models. While the controversy may not be solved easily, a critical question is whether mitochondrial fragmentation occurs in vivo under disease conditions and how much it contributes to pathological apoptosis. Unfortunately, examination of mitochondrial fragmentation in vivo in mammalian tissues is not a trivial task. Thus far, the only reported examination is from Barsoum et al., who showed that mitochondria were fragmented in neurons in ischemically injured brain (26). However, whether the fragmentation is important to neuronal apoptosis in the brain was not determined. Our current study has demonstrated convincing evidence for mitochondrial fragmentation in kidneys following ischemia/reperfusion by using 2D and 3D EM. Importantly, we have further shown that pharmacological blockade of mitochondrial fission can attenuate tubular cell apoptosis, tissue damage, and renal injury, demonstrating what we believe is the first in vivo evidence for a role of the regulation of mitochondrial morphological dynamics in pathological apoptosis in disease models.

Of note, in many tissue types, mitochondria are randomly oriented and, as a result, tissue sectioning for EM results in cross sections of most mitochondria within a cell. These mitochondria would then appear to be small and round, difficult to distinguish from fragmented mitochondria in 2D EM. In this regard, tubular cells in the kidneys make an excellent model for studying mitochondrial fragmentation in vivo because in these cells a significant portion of mitochondria line up perpendicular to the basement membrane and, as a result, cross sections of tubules would normally reveal 10%–20% longitudinally sectioned long mitochondria in a given cell. In contrast, when mitochondria are fragmented, they appear as short rods or spherical fragments, no matter how they are sectioned. The unique feature of mitochondrial organization in renal tubular cells not only makes it easier to count and quantify mitochondria-fragmented cells but also ensures the reliability of the results. In this study, we have further verified the 2D EM results by 3D reconstruction of serial section EM images.

The morphology of mitochondria is determined by a balance between fission and fusion (20–22). Thus, fragmentation of the organelles can be a result of increased fission, suppressed fusion, or a combination of both. In this study, during renal tubular cell injury, we detected an early activation and mitochondrial translocation of Drp1, a critical fission protein. Moreover, suppression of Drp1 by dominant-negative mutants, siRNA, or mdivi-1 can block mitochondrial fragmentation. These results, though not excluding a role for mitochondrial fusion regulation, suggest that mitochondrial fission is activated under experimental conditions and contributes to the observed mitochondrial fragmentation. It is unclear how Drp1 is activated. Posttranslational modification of Drp1 including phosphorylation and sumoylation has been documented and may play a role in Drp1 activation upon apoptotic stress (36, 37). Further investigations should examine these possibilities during renal cell injury. In addition, Drp1 is also involved in the fission of peroxisomes (38, 39). Whether and to what extent Drp1-related changes in peroxisomes contribute to mitochondrial damage and apoptosis has yet to be determined.

It is currently unclear how mitochondrial fragmentation, a seemingly morphological change, can have an impact on mitochondrial membrane permeabilization (18, 19). It is clear from previous studies

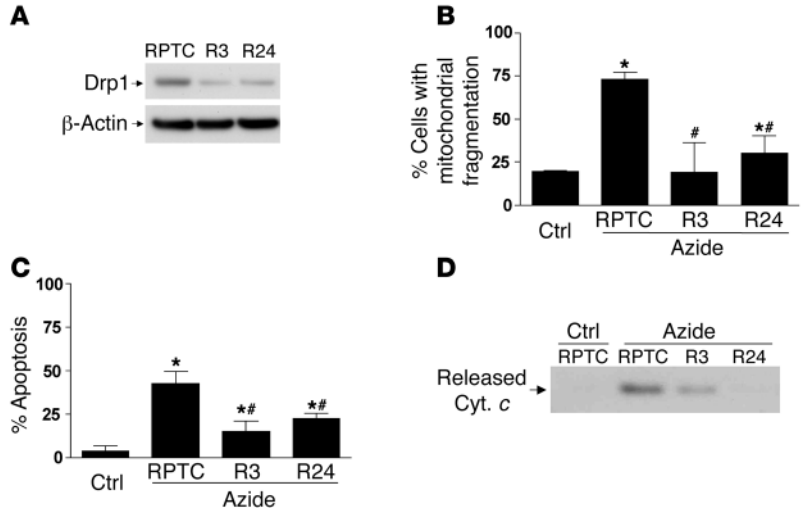

Figure 7

siRNA knockdown of Drp1 inhibits mitochondrial fragmentation, cytochrome *c* release, and apoptosis following ATP depletion in RPTCs. (**A**) RPTCs were transfected with Drp1 short hairpin siRNA to select 2 stable cell lines: R3 and R24. Knockdown of Drp1 in R3 and R24 cells was verified by immunoblot analysis. (**B**) RPTCs, R3 cells, and R24 cells were transfected with MitoRed and then incubated with 10 mM azide for 3 hours. Cells were examined by fluorescence microscopy to enable counting of cells with mitochondrial fragmentation. (**C**) RPTCs, R3 cells, and R24 cells were incubated with 10 mM azide for 3 hours followed by 2 hours recovery to evaluate apoptosis by morphological criteria. (**D**) RPTCs, R3 cells, and R24 cells were incubated with 10 mM azide for 3 hours. Cells were then fractionated to collect the cytosolic fraction for immunoblot analysis of cytochrome *c*. Data in **B** and **C** are presented as mean ± SD; $n \geq 3$. $^{*}P < 0.05$, significantly different from untreated control RPTCs; $^{\#}P < 0.05$, significantly different from azide-treated RPTCs.

that mitochondrial fragmentation alone is not effective or sufficient to trigger porous defects in the outer membrane (18, 19). In support, our recent work showed that although all apoptotic cells have fragmented mitochondria, not all mitochondria-fragmented cells have cytochrome *c* release or apoptosis (40). We further showed that fragmented mitochondria can re-fuse if the injurious stress is removed before permanent damage occurs to trigger apoptosis (our unpublished observations). However, when the injury is prolonged, mitochondria cannot re-fuse and become irreversibly damaged. These observations suggest that mitochondrial fragmentation is not the "point of no return"; rather, it is a facilitating event for irreversible damage. It is likely that fragmentation sensitizes mitochondria to additional injurious events, which precipitate in the membrane leakage. One such event, as proposed in our recent work (40), is initiated and mediated by Bax and Bak. Mitochondrial fragmentation is virtually a process of membrane bending, scission, and remelding. The associated biochemical and biophysical changes of the membrane are expected to significantly affect the interaction, activation, and function of the molecules residing in or accumulating near the membrane. Mitochondrial outer membrane permeabilization involves the activation of Bax and Bak and significant conformational changes of the proteins (41–45). Thus, fragmentation may predispose the mitochondria to Bax/Bak-induced development of porous defects. This scenario, also called the "2-hit" hypothesis (46), emphasizes 2 critical events of outer membrane permeabilization: mitochondrial fragmentation and Bax/Bak-mediated pore formation. It is noteworthy that these 2 events are not separately regulated, as both may be subjected to regulation by Bcl2 family proteins (18, 46).

Our present results show that temporary blockade of fission can prevent mitochondrial fragmentation and tubular cell apoptosis during acute kidney injury. However, it is important to note that permanent blockade of mitochondrial fission may adversely affect mitochondrial, cellular, and renal function or physiology. In this regard, Chan and colleagues showed that mitochondrial fragmentation due to loss of fusion proteins leads to defects in mitochondrial respiration and oxygen consumption accompanied by loss of mitochondrial membrane potential and cell growth inhibition (47). Interestingly, Rossignol and colleagues demonstrated that forced fusion of mitochondria by Drp1 knockdown also results in a reduction in respiration and oxygen consumption (48). These results, seemingly contradictory, suggest that mitochondrial morphological dynamics is a key to mitochondrial physiology and perturbation of the dynamics to either fission or fusion direction would reduce mitochondrial function.

In conclusion, this study has demonstrated mitochondrial fragmentation in both ischemic and nephrotoxic models of acute renal failure. Mitochondrial fragmentation occurs early and contributes to subsequent development of mitochondrial membrane permeabilization, release of apoptogenic factors, and tubular cell apoptosis. Importantly, inhibition of mitochondrial fragmentation protects against tubular cell apoptosis and renal injury, suggesting what we believe is a novel strategy for the prevention and treatment of acute renal failure.

Methods

Antibodies, plasmids, and other reagents. Antibodies and sources are as follows: monoclonal anti–cytochrome *c* (7H8.2C12 and 6H2.B4), anti-active caspase-3, and anti-Drp1 from BD Biosciences — Pharmingen; polyclonal anti-Fis1 from ALEXIS Biochemicals; polyclonal anti–phospho-p53 from Cell Signaling Technology; monoclonal anti-Bax from NeoMarkers; polyclonal anti-PUMA from Jian Yu (University of Pittsburgh, Pittsburgh, Pennsylvania, USA); and all secondary antibodies from Jackson ImmunoResearch Laboratories Inc. Plasmids containing Drp1 or its dominant-negative mutant were kindly provided by Alexander van der Bliek (UCLA School of Medicine, Los Angeles, California, USA) (28) and were further subcloned into pcDNA3.1 (Invitrogen) for this study. The short hairpin Drp1 siRNA plasmid was a gift from Ansgar Santel (Silence Therapeutics, Berlin, Germany) (30). pDsRed2-Mito (MitoRed), an expression vector encoding red fluorescent protein with a mitochondrial targeting sequence, was purchased from Clontech. All other reagents were purchased from Sigma-Aldrich unless otherwise noted.

RPTC lines. RPTCs were originally provided by Ulrich Hopfer (Case Western Reserve University, Cleveland, Ohio, USA). RPTC lines stably transfected with Bcl2 were generated in previous work (49). RPTC lines with Drp1 knockdown were generated by transfection with the short hairpin Drp1 siRNA plasmid (30), followed by hygromycin selection. In brief, RPTCs were cotransfected with the Drp1 siRNA plasmid and a hygromycin resistance vector. 24 hours after transfection, cells were treated with 400 μg/ml hygromycin (Sigma-Aldrich). Hygromycin treatment was continued until the original monolayer of cells was reduced to individual cells. The hygromycin concentration was then reduced to 200 μg/ml to allow the individual cells to proliferate into colonies. Individual colonies were extracted and cultured,

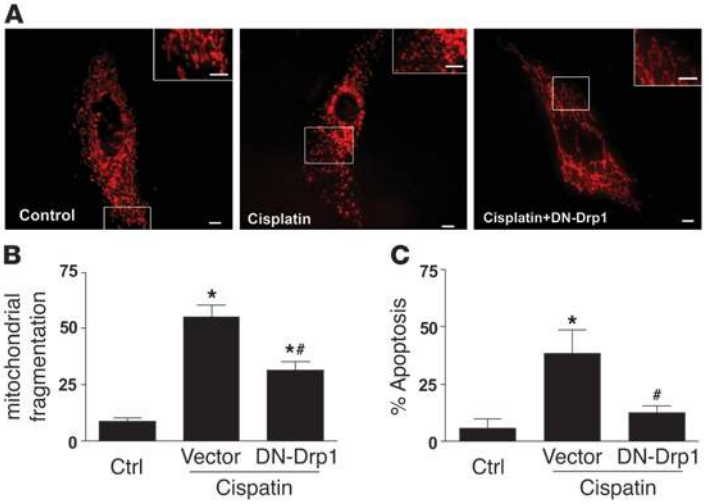

Figure 8
Mitochondrial fragmentation and its inhibition by DN-Drp1 in primary cultures of proximal tubular cells. Proximal tubular cells were isolated from renal cortex of male C57BL/6 mice for primary culture. Primary cells were cotransfected with MitoRed and DN-Drp1 or empty vector. Cells were then incubated with 50 μM cisplatin for 24 hours. Mitochondrial morphology was examined by fluorescence microscopy. Apoptosis in transfected cells was evaluated by morphological criteria. (**A**) Representative mitochondrial morphology. Scale bars: 5 μm. Insets show higher magnification of the framed areas. (**B**) Effects of DN-Drp1 on mitochondrial fragmentation. (**C**) Effects of DN-Drp1 on apoptosis. Data in **B** and **C** are presented as mean ± SD; $n \geq 3$. $^{*}P < 0.05$, significantly different from untreated control; $^{\#}P < 0.05$, significantly different from cisplatin-treated vector-transfected cells.

then tested for Drp1 expression. All RPTCs were maintained in Ham's F-12/DMEM supplemented with 10% FBS, 5 μg/ml transferrin, 5 μg/ml insulin, 1 ng/ml EGF, 4 μg/ml dexamethasone, and 1% antibiotics.

Primary renal proximal tubular cells. C57BL/6 mice (8 to 12 weeks, male) were purchased from The Jackson Laboratory. Renal cortical tissues were harvested from animals to isolate proximal tubular cells for culture as previously described (15, 33). In brief, cortical tissues were minced, digested with collagenase, and centrifuged in 32% Percoll medium to purify proximal tubular cells. Cells were then plated in collagen-coated dishes and maintained in DMEM/F-12 medium supplemented with 5 μg/ml transferrin, 5 μg/ml insulin, 0.05 μM hydrocortisone, and 50 μM vitamin C.

Apoptotic treatment. For ATP depletion, cells were treated with 10 mM azide in glucose-free Krebs-Ringer bicarbonate solution for 3 hours or time as indicated (50). After the incubation, cells were fractionated for analysis of cytochrome *c* release, fixed for immunostaining and microscopic examination, or returned to glucose-containing culture medium for 2 hours to observe apoptosis (51, 52). For cisplatin treatment, RPTC lines were incubated with 20 μM cisplatin in culture medium for 4 to 16 hours (53), whereas primary mouse kidney tubular cells were incubated with 50 μM cisplatin for 20 hours (15).

Transfection. RPTCs were plated at approximately 50% confluence and transfected with 1.0 μg plasmid DNA using Lipofectamine PLUS reagent (Invitrogen). Primary cultures of isolated kidney tubular cells were plated at approximately 70% confluence for transfection with 1.0 μg plasmid DNA using Lipofectamine 2000 according to the manufacturer's instructions (Invitrogen). To visualize mitochondria, cells were transfected with 0.1 μg pDsRed2-Mito to label mitochondria with the red fluorescent MitoRed protein.

Mitochondrial and cell morphology. Mitochondrial morphology was examined by fluorescence microscopy in pDsRed2-Mito–transfected cells as described in our recent study (40). pDsRed2-Mito transfection leads to the expression in mitochondria of the red fluorescent protein MitoRed, a fusion protein containing a red fluorescent sequence and a mitochondrial targeting domain of cytochrome *c* oxidase, subunit VIII. MitoRed signal is not sensitive to changes of mitochondrial conditions including membrane potential and redox status. In brief, cells were transfected with pDsRed2-Mito. After various treatments, the cells were examined by fluorescence microscopy to evaluate mitochondrial morphology in individual cells. Mitochondria of untreated cells were filamentous and showed a threadlike tubular structure, while mitochondria in stressed cells were fragmented and appeared shortened and punctate. Consistent with earlier studies (15, 54, 55), the mitochondria within a cell were often either filamentous or fragmented. In uncommon cases of mixed mitochondrial morphology, we classified the cells based on the majority (>70%) of mitochondria. Cytochrome *c* release and apoptotic morphology were often evaluated in the same cells that were assessed for mitochondrial morphology. Cytochrome *c* release was indicated by the loss of mitochondrial cytochrome *c* staining and the appearance of cytochrome *c* in cytosol. Typical apoptotic morphology was indicated by cellular condensation, formation of apoptotic bodies, and condensation and fragmentation of the nucleus. For each sample, several random fields of cells (≥100 cells per dish) were evaluated for mitochondrial morphology, apoptosis, and cytochrome *c* release.

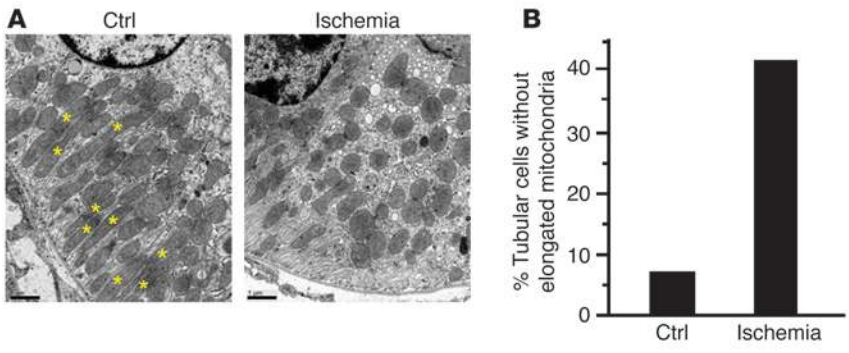

Figure 9
2D EM analysis of mitochondrial fragmentation in kidney tissues. C57BL/6 mice (male, ~8 weeks) were subjected to 30 minutes of bilateral renal ischemia followed by 15 minutes of reperfusion (Ischemia) or control sham operation (Ctrl). Kidneys were fixed in situ via vascular perfusion and processed for EM. (**A**) EM micrographs of a control and an ischemically injured proximal tubular cell. Scale bars: 1 μm. Asterisks indicate elongated (>2 μm) mitochondria. (**B**) Quantification of mitochondrial fragmentation. Mitochondrial length was measured in individual tubular cells to determine the percentage of cells that showed filamentous mitochondria less than 1% long (>2 μm). A total of 90 cells in control and 160 cells in ischemic kidneys from 4 animals were evaluated.

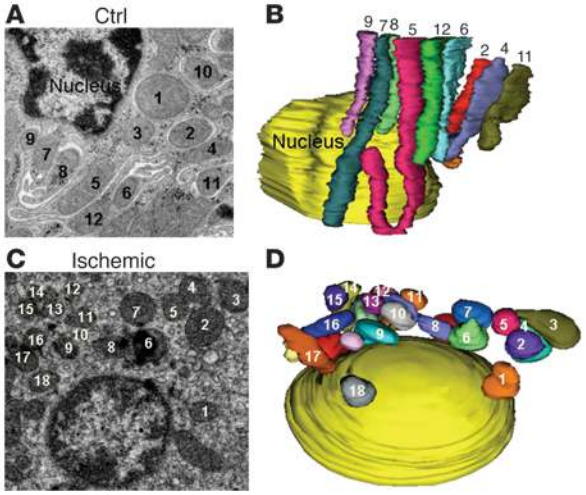

Figure 10
3D image of mitochondria in control and ischemically injured tubular cells. C57BL/6 mice (male, ~8 weeks) were subjected to 30 minutes of bilateral renal ischemia followed by 15 minutes of reperfusion or control sham operation. Kidneys were fixed in situ via vascular perfusion and processed to collect 100 serial sections of a representative region at 45 nm/section for EM. EM micrographs of serial section no. 50 were shown for 2D image. For 3D image, EM images of the 100 serial sections were aligned for 3D reconstruction using the Reconstruct software. (**A**) 2D EM image of a control tubular cell. (**B**) 3D EM image of the same control cell as shown in **A**. (**C**) 2D EM image of an ischemically injured tubular cell. (**D**) 3D EM image of the same ischemic cell as shown in **C**. Note: The numbered mitochondria shown in **A** and **B** correspond respectively with those in **C** and **D**. In addition, some numbered mitochondria in 2D images are masked in the 3D images.

Immunofluorescence and TUNEL staining. Cells were grown on collagen-coated glass coverslips and subjected to various treatments. The cells were then fixed with a modified Zamboni's fixative containing 4% paraformaldehyde and picric acid and permeabilized with 0.1% SDS. Cells were blocked with 5% normal goat serum and 2% BSA. After blocking, cells were incubated with primary antibodies (monoclonal mouse anti–cytochrome *c*, anti-Drp1, anti-Fis1, or anti-active caspase-3) and secondary antibodies (Cy-3–labeled or FITC-labeled goat anti-mouse IgG). TUNEL staining was performed using the *In Situ* Cell Death Detection Kit from Roche Applied Science according to the manufacturer's instructions. In brief, cells were grown on collagen-coated glass coverslips for experiment, then fixed with 4% paraformaldehyde and permeabilized with 0.1% Triton X-100 in 0.1% sodium citrate. Cells were then incubated with the TUNEL reaction mixture for 1 hour at 37°C. Immunofluorescence and TUNEL staining were examined by fluorescence and confocal microscopy, using a LSM 510 Zeiss microscope.

Cellular fractionation. To study cytochrome *c* release, cells were incubated with 0.05% digitonin in an isotonic sucrose buffer (250 mM sucrose, 10 mM HEPES-NaOH, 10 mM KCl, 1.5 mM $MgCl_2$, 1 mM EDTA, 1 mM EGTA, and 0.5 mM phenylmethylsulfonyl fluoride; pH 7.2) at room temperature as described previously (40, 49). At this concentration, digitonin selectively permeabilizes the plasma membrane but not the mitochondrial membrane. The digitonin extract was collected as the cytosolic fraction for immunoblot analysis. To examine Drp1 translocation to mitochondria during apoptosis, cells were collected in ice-cold isotonic sucrose buffer by gentle scraping. The cells were then homogenized with a Wheaton homogenizer. The homogenate was centrifuged at 1000 *g* to remove debris and nuclei to collect the supernatant for further

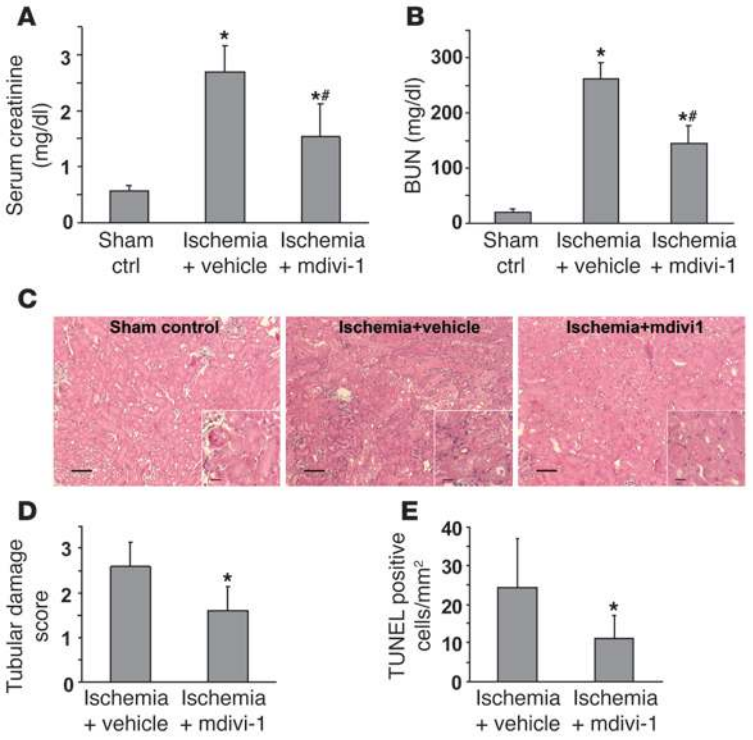

Figure 11
Amelioration of ischemic renal injury and tubular apoptosis by mdivi-1, a pharmacological inhibitor of Drp1. C57BL/6 mice were injected with 50 mg/kg mdivi-1 or vehicle solution for 1 hour and then subjected to 30 minutes of bilateral renal ischemia followed by 48 hours of reperfusion. Control animals were subjected to sham operation without renal ischemia. Blood samples and renal tissues were collected for analysis. (**A**) Serum creatinine. (**B**) BUN. (**C**) Representative renal histology. Insets show higher magnification. Scale bars: 80 μm; 20 μm (insets). (**D**) Quantification of tubular damage. The percentage of damaged renal tubules was determined for each animal for histology scoring as described in Methods. (**E**) Tubular apoptosis. Renal tissues were subjected to TUNEL assay to enable counting positive cells to indicate apoptosis. Data are presented as mean ± SD; $n \geq 5$. $^{*}P < 0.05$, significantly different from sham control. $^{\#}P < 0.05$, significantly different from ischemic group injected with vehicle solution.

centrifugation at 10,000 *g* to yield the mitochondrial fraction. Homogenization and centrifugation procedures were conducted at 4°C.

Immunoblot analysis. Standard procedure was performed for immunoblotting using NuPAGE (Invitrogen) or Bio-Rad Gel Systems. In brief, 25 μg protein from each sample was resolved by SDS-PAGE electrophoresis under reducing conditions. Proteins were then transferred to PVDF membranes and blocked using 5% milk. The membranes were then incubated with primary antibody overnight at 4°C and with HRP-conjugated secondary antibodies for 1 hour at room temperature. The antigen-specific signal was then detected through incubation with enhanced chemoluminescence substrate (Pierce Biotechnology).

Renal ischemia/reperfusion in C57BL/6 mice. C57BL/6 mice purchased from The Jackson Laboratory were maintained in the animal facility of Charlie Norwood VA Medical Center at Augusta under a 12-hour light/12-hour dark cycle with free access to food and water. Renal ischemia was induced in male mice of 8 to 10 weeks as described previously (15, 16, 33). In brief, the animals were anesthetized with pentobarbital (i.p., 50 mg/kg) and were kept on a homeothermic table. Flank incisions were made to expose the renal pedicles for bilateral clamping to induce 30 minutes of renal ischemia. The clamps were then released for reperfusion for indicated times. Control animals were subjected to sham operation without renal pedicle clamping. To test the effects of mdivi-1, the animals were injected (i.p.) with 50 mg/kg body weight mdivi-1 1 hour prior to renal ischemia/reperfusion. All experiments involving animals were conducted according to a protocol approved by the Institutional Animal Care and Use Committees of Charlie Norwood VA Medical Center.

Renal function, histology, and TUNEL assay. Serum creatinine and BUN were determined to monitor renal function as previously reported (15, 16, 33). For histology, kidneys were fixed with 4% paraformaldehyde, paraffin embedded, and stained with H&E. Histopathological changes evaluated in this study included loss of brush border, tubular dilation, cast formation, and cell lysis. Tissue damage was examined in a blind manner and scored according to the percentage of damaged tubules: 0, no damage; 1, less than 25% damage; 2, 25%–50% damage; 3, 50%–75% damage; and 4, more than 75% damage. TUNEL assay was performed to evaluate apoptosis in renal tissues using the *In Situ* Cell Death Detection Kit from Roche Applied Science as described previously (15, 16, 33). In brief, renal tissues were fixed with 4% paraformaldehyde and paraffin embedded. Tissue sections of 4 μm were exposed to a TUNEL reaction mixture containing terminal deoxynucleotidyl transferase and nucleotides, including tetramethylrhodamine–labeled (TMR-labeled) dUTP. The slides were examined by fluorescence microscopy.

Examination of mitochondrial fragmentation in renal tissues by 2D EM. Sham-operated control and ischemia/reperfused animals were perfused with 10 ml (at 10 units/ml) heparin, followed by 50 ml fixative containing 100 mM sodium cacodylate, 2 mM $CaCl_2$, 4 mM $MgSO_4$, 4% paraformaldehyde, and 2.5% glutaraldehyde. Kidneys were then harvested and postfixed in the same fixative. A tissue block of approximately 1 mm^3 was collected from each kidney, including a portion of renal cortex and outer medulla for standard processing for EM. The tissue block was examined initially at low magnification (×3,000) to identify representative proximal tubules. Cells in these tubules were then examined at high magnification (×15,000) to reveal mitochondria. To determine mitochondrial fragmentation, digital images with scale bars were collected in EM. The lengths of individual mitochondria in a cell were measured by tracing using NIH ImageJ software (http://rsbweb.nih.gov/ij/). For each cell, approximately 100 mitochondria in a representative area were measured to determine the percentage distribution of mitochondria with various lengths (0–1 μm, 1–2 μm, >2 μm). We showed that the mitochondrial diameter of tubular cells is approximately 0.3 to 0.5 μm and that a mitochondrion with length greater than 2 μm is clearly filamentous (Figure 9). In 2D EM, proximal tubular cells in control tissues consistently showed 10%–20% long filamentous mitochondria. If a cell had undergone mitochondrial fragmentation, then very few or no filamentous mitochondria would appear. Thus, we determined the percentage of cells that had less than 1% long filamentous mitochondria to indicate the degree of mitochondrial fragmentation.

Examination of mitochondria in renal tissues by 3D EM. Renal tissues were fixed and processed for EM as described above. The tissues were initially examined to identify representative proximal tubules for serial section. One hundred serial sections (45 nm/section) were collected from representative tubules or cells. EM images of the serial sections were obtained and then aligned to reconstruct a 3D image of mitochondria using Reconstruct Software, version 1.1.0.0 (http://synapses.clm.utexas.edu/tools/reconstruct/reconstruct.stm).

Statistics. Quantitative data were expressed as mean ± SD from at least 3 separate experiments. Statistical differences between the means were determined using ANOVA followed by Tukey's post test. $P < 0.05$ was considered significant. Qualitative data including cell images and immunoblots are representative of at least 3 separate experiments.

Acknowledgments

We thank Alexander van der Bliek (University of California School of Medicine, Los Angeles, California, USA) and Ansgar Santel (Silence Therapeutics, Berlin, Germany) for providing plasmids. We also thank Robert Smith and Libby Perry at the Electron Microscopy Core Laboratory of the Medical College of Georgia for their assistance with electron microscopy in this study. Craig Brooks was supported in part by the Multidisciplinary Predoctoral Training Program in Integrative Cardiovascular Biology from the NIH. Zheng Dong is a Research Career Scientist at the United States Department of Veterans Affairs (VA). The study was supported by grants from the NIH and the VA.

Received for publication October 21, 2008, and accepted in revised form February 18, 2009.

Address correspondence to: Zheng Dong, Department of Cellular Biology and Anatomy, Medical College of Georgia, 1459 Laney Walker Blvd., Augusta, Georgia 30912, USA. Phone: (706) 721-2825; Fax: (706) 721-6120; E-mail: zdong@mail.mcg.edu.

Craig Brooks's present address is: Renal Division, Department of Medicine, Brigham and Women's Hospital, Harvard Medical School, Boston, Massachusetts, USA.

1. Bonventre, J.V., and Weinberg, J.M. 2003. Recent advances in the pathophysiology of ischemic acute renal failure. *J. Am. Soc. Nephrol.* **14**:2199–2210.
2. Lieberthal, W., and Nigam, S.K. 1998. Acute renal failure. I. Relative importance of proximal vs. distal tubular injury. *Am. J. Physiol.* **275**:F623–F631.
3. Devarajan, P. 2006. Update on mechanisms of ischemic acute kidney injury. *J. Am. Soc. Nephrol.***17**:1503–1520.
4. Molitoris, B.A. 2003. Transitioning to therapy in ischemic acute renal failure. *J. Am. Soc. Nephrol.* **14**:265–267.
5. Lieberthal, W., and Nigam, S.K. 2000. Acute renal failure. II. Experimental models of acute renal failure: imperfect but indispensable. *Am. J. Physiol. Renal Physiol.* **278**:F1–F12.
6. Pabla, N., and Dong, Z. 2008. Cisplatin nephrotoxicity: Mechanisms and renoprotective strategies. *Kidney Int.* **73**:994–1007.
7. Schrier, R.W., Wang, W., Poole, B., and Mitra, A. 2004. Acute renal failure: definitions, diagnosis, pathogenesis, and therapy. *J. Clin. Invest.* **114**:5–14.
8. Waikar, S.S., Curhan, G.C., Wald, R., McCarthy, E.P., and Chertow, G.M. 2006. Declining mortality in patients with acute renal failure, 1988 to 2002. *J. Am. Soc. Nephrol.* **17**:1143–1150.
9. Xue, J.L., et al. 2006. Incidence and mortality of

acute renal failure in Medicare beneficiaries, 1992 to 2001. *J. Am. Soc. Nephrol.* **17**:1135–1142.
10. Kaushal, G.P., Basnakian, A.G., and Shah, S.V. 2004. Apoptotic pathways in ischemic acute renal failure. *Kidney Int.* **66**:500–506.
11. Padanilam, B.J. 2003. Cell death induced by acute renal injury: a perspective on the contributions of apoptosis and necrosis. *Am. J. Physiol. Renal Physiol.* **284**:F608–F627.
12. Weinberg, J.M. 1991. The cell biology of ischemic renal injury. *Kidney Int.* **39**:476–500.
13. Sanz, A.B., Santamaria, B., Ruiz-Ortega, M., Egido, J., and Ortiz, A. 2008. Mechanisms of renal apoptosis in health and disease. *J. Am. Soc. Nephrol.* **19**:1634–1642.
14. Servais, H., et al. 2008. Renal cell apoptosis induced by nephrotoxic drugs: cellular and molecular mechanisms and potential approaches to modulation. *Apoptosis.* **13**:11–32.
15. Wei, Q., Dong, G., Franklin, J., and Dong, Z. 2007. The pathological role of Bax in cisplatin nephrotoxicity. *Kidney Int.* **72**:53–62.
16. Wei, Q., Yin, X.M., Wang, M.H., and Dong, Z. 2006. Bid deficiency ameliorates ischemic renal failure and delays animal death in C57BL/6 mice. *Am. J. Physiol. Renal Physiol.* **290**:F35–F42.
17. Castaneda, M.P., et al. 2003. Activation of mitochondrial apoptotic pathways in human renal allografts after ischemiareperfusion injury. *Transplantation.* **76**:50–54.
18. Suen, D.F., Norris, K.L., and Youle, R.J. 2008. Mitochondrial dynamics and apoptosis. *Genes Dev.* **22**:1577–1590.
19. Herzig, S., and Martinou, J.C. 2008. Mitochondrial dynamics: to be in good shape to survive. *Curr. Mol. Med.* **8**:131–137.
20. Chan, D.C. 2006. Mitochondrial fusion and fission in mammals. *Annu. Rev. Cell Dev. Biol.* **22**:79–99.
21. Okamoto, K., and Shaw, J.M. 2005. Mitochondrial morphology and dynamics in yeast and multicellular eukaryotes. *Annu. Rev. Genet.* **39**:503–536.
22. Westermann, B. 2008. Molecular machinery of mitochondrial fusion and fission. *J. Biol. Chem.* **283**:13501–13505.
23. Breckenridge, D.G., et al. 2008. Caenorhabditis elegans drp-1 and fis-2 regulate distinct cell-death execution pathways downstream of ced-3 and independent of ced-9. *Mol. Cell.* **31**:586–597.
24. James, D.I., and Martinou, J.C. 2008. Mitochondrial dynamics and apoptosis: a painful separation. *Dev. Cell.* **15**:341–343.
25. Sheridan, C., Delivani, P., Cullen, S.P., and Martin, S.J. 2008. Bax- or Bak-induced mitochondrial fission can be uncoupled from cytochrome C release. *Mol. Cell.* **31**:570–585.
26. Barsoum, M.J., et al. 2006. Nitric oxide-induced mitochondrial fission is regulated by dynamin-related GTPases in neurons. *EMBO J.* **25**:3900–3911.
27. Karbowski, M., et al. 2002. Spatial and temporal association of Bax with mitochondrial fission sites, Drp1, and Mfn2 during apoptosis. *J. Cell Biol.* **159**:931–938.
28. Smirnova, E., Griparic, L., Shurland, D.L., and van der Bliek, A.M. 2001. Dynamin-related protein Drp1 is required for mitochondrial division in mammalian cells. *Mol. Biol. Cell.* **12**:2245–2256.
29. Wang, X. 2001. The expanding role of mitochondria in apoptosis. *Genes Dev.* **15**:2922–2933.
30. Tondera, D., et al. 2005. The mitochondrial protein MTP18 contributes to mitochondrial fission in mammalian cells. *J. Cell Sci.* **118**:3049–3059.
31. Jiang, M., et al. 2006. Regulation of PUMA-alpha by p53 in cisplatin-induced renal cell apoptosis. *Oncogene.* **25**:4056–4066.
32. Cassidy-Stone, A., et al. 2008. Chemical inhibition of the mitochondrial division dynamin reveals its role in Bax/Bak-dependent mitochondrial outer membrane permeabilization. *Dev. Cell.* **14**:193–204.
33. Wei, Q., et al. 2007. Activation and involvement of p53 in cisplatin-induced nephrotoxicity. *Am. J. Physiol. Renal Physiol.* **293**:F1282–F1291.
34. Perfettini, J.L., Roumier, T., and Kroemer, G. 2005. Mitochondrial fusion and fission in the control of apoptosis. *Trends Cell Biol.* **15**:179–183.
35. Jagasia, R., Grote, P., Westermann, B., and Conradt, B. 2005. DRP-1-mediated mitochondrial fragmentation during EGL-1-induced cell death in C. elegans. *Nature.* **433**:754–760.
36. Cribbs, J.T., and Strack, S. 2007. Reversible phosphorylation of Drp1 by cyclic AMP-dependent protein kinase and calcineurin regulates mitochondrial fission and cell death. *EMBO Rep.* **8**:939–944.
37. Wasiak, S., Zunino, R., and McBride, H.M. 2007. Bax/Bak promote sumoylation of DRP1 and its stable association with mitochondria during apoptotic cell death. *J. Cell Biol.* **177**:439–450.
38. Waterham, H.R., et al. 2007. A lethal defect of mitochondrial and peroxisomal fission. *N. Engl. J. Med.* **356**:1736–1741.
39. Schrader, M. 2006. Shared components of mitochondrial and peroxisomal division. *Biochim. Biophys. Acta.* **1763**:531–541.
40. Brooks, C., et al. 2007. Bak regulates mitochondrial morphology and pathology during apoptosis by interacting with mitofusins. *Proc. Natl. Acad. Sci. U. S. A.* **104**:11649–11654.
41. Adams, J.M., and Cory, S. 2001. Life-or-death decisions by the Bcl-2 protein family. *Trends Biochem. Sci.* **26**:61–66.
42. Danial, N.N., and Korsmeyer, S.J. 2004. Cell death: critical control points. *Cell.* **116**:205–219.
43. Harris, M.H., and Thompson, C.B. 2000. The role of the Bcl-2 family in the regulation of outer mitochondrial membrane permeability. *Cell Death Differ.* **7**:1182–1191.
44. Martinou, J.C., and Green, D.R. 2001. Breaking the mitochondrial barrier. *Nat. Rev. Mol. Cell Biol.* **2**:63–67.
45. Youle, R.J., and Strasser, A. 2008. The BCL-2 protein family: opposing activities that mediate cell death. *Nat. Rev. Mol. Cell Biol.* **9**:47–59.
46. Brooks, C., and Dong, Z. 2007. Regulation of mitochondrial morphological dynamics during apoptosis by Bcl-2 family proteins: a key in Bak? *Cell Cycle.* **6**:3043–3047.
47. Chen, H., Chomyn, A., and Chan, D.C. 2005. Disruption of fusion results in mitochondrial heterogeneity and dysfunction. *J. Biol. Chem.* **280**:26185–26192.
48. Benard, G., et al. 2007. Mitochondrial bioenergetics and structural network organization. *J. Cell Sci.* **120**:838–848.
49. Saikumar, P., et al. 1998. Role of hypoxia-induced Bax translocation and cytochrome c release in reoxygenation injury. *Oncogene.* **17**:3401–3415.
50. Brooks, C., Wang, J., Yang, T., and Dong, Z. 2007. Characterization of cell clones isolated from hypoxia-selected renal proximal tubular cells. *Am. J. Physiol. Renal Physiol.* **292**:F243–F252.
51. Dong, Z., and Wang, J. 2004. Hypoxia selection of death-resistant cells: a role for Bcl-XL. *J. Biol. Chem.* **279**:9215–9221.
52. Wang, J., et al. 2004. Minocycline up-regulates Bcl-2 and protects against cell death in mitochondria. *J. Biol. Chem.* **279**:19948–19954.
53. Pabla, N., Huang, S., Mi, Q.S., Daniel, R., and Dong, Z. 2008. ATR-Chk2 signaling in p53 activation and DNA damage response during cisplatin-induced apoptosis. *J. Biol. Chem.* **283**:6572–6583.
54. Youle, R.J., and Karbowski, M. 2005. Mitochondrial fission in apoptosis. *Nat. Rev. Mol. Cell Biol.* **6**:657–663.
55. Lee, Y.J., Jeong, S.Y., Karbowski, M., Smith, C.L., and Youle, R.J. 2004. Roles of the mammalian mitochondrial fission and fusion mediators Fis1, Drp1, and Opa1 in apoptosis. *Mol. Biol. Cell.* **15**:5001–5011.